Applied Catalysis B: Environmental 201 (2017) 22–28

Contents lists available at ScienceDirect

Applied Catalysis B: Environmental

journal homepage: www.elsevier.com/locate/apcatb

NiO_x-Pt/C nanocomposites: Highly active electrocatalysts for the electrochemical oxidation of hydrazine

Drielly C. de Oliveira [a], Wanderson O. Silva [a], Marian Chatenet [b,c,d], Fabio H.B. Lima [a,*]

[a] Instituto de Química de São Carlos, Universidade de São Paulo, CEP 13560-970, CP 780, São Carlos, SP, Brazil
[b] Univ. Grenoble Alpes, LEPMI, F-38000 Grenoble, France
[c] CNRS, LEPMI, F-38000 Grenoble, France
[d] Institut Universitaire de France, IUF, Paris, France

ARTICLE INFO

Article history:
Received 13 June 2016
Received in revised form 1 August 2016
Accepted 2 August 2016
Available online 3 August 2016

Keywords:
Hydrazine electrooxidation
Nickel-platinum electrocatalyst
On-line DEMS
Alkaline fuel cells

ABSTRACT

NiO_x-modified Pt/C nanocomposites are synthesized and investigated for hydrazine electrooxidation in an alkaline electrolyte. The reaction onset potential is significantly reduced in comparison to that of pure Pt/C, owing to the occurrence of a bifunctional mechanism, in which OH species on Ni sites facilitate the oxidation of adsorbed H atoms on the Pt surface. On-line Differential Electrochemical Mass Spectrometry (DEMS) shows that NiO_x-Pt/C catalyzes the heterogeneous chemical hydrolysis at open circuit potential, producing H_2 and N_2. Just above the OCP, the H_2 signal in DEMS decreases concomitantly with the increase in faradaic current, due to quantitative H_2 (and H_{ad}) electrooxidation on Pt, or due to the deceleration of the overall reaction of hydrolysis. At slightly higher potentials, the N_2 signal further rises, which indicates the onset of complete electrooxidation of hydrazine. In the platinum-oxide region, the H_2 signal increases again and this process is also accompanied by a small ionic signal of NH_3, evidencing the occurrence of an incomplete hydrazine electrooxidation route, at least in a minor extent.

© 2016 Elsevier B.V. All rights reserved.

1. Introduction

The research related to energy conversion technologies has increased in the last decades. Among these technologies, fuel cells have attracted attention, mainly because of their high performance. Particularly, for energy supply of space and underwater (air-independent) or other specific vehicles, fuel cells powered by compounds with high hydrogen content such as borohydride, hydrazine or their derivatives, take benefit of their higher volumetric energy densities, in comparison to that of molecular hydrogen [1,2]. These compounds can be directly employed as fuels [3–5] in different fuel cell configurations; for example: hydrazine/hydrogen peroxide (air-independent) [2], hydrazine/air, using cation and anion exchange membranes, respectively [6–8], and membraneless hydrazine/air fuel cells [2,8,9]. Alternatively, hydrazine (or borohydride) can be electrochemically oxidized for H_2 production in electrochemical reformers for H_2/air fuel cells [10,11].

Hydrazine presents a low standard potential value ($E^0 = -0.33$ V *vs* RHE), and its desired electrooxidation product is N_2 (Eq. (1)), which is neither harmful to the environment nor toxic. An additional benefit of hydrazine is the possibility of its safe storage in solid polymers with carbonyl or amide groups.

$$N_2H_4 + 4OH^- \rightarrow N_2 + 4H_2O + 4e^- \quad (E^0 = -0.33\,V\,vs\,RHE) \quad (1)$$

Platinum is an effective electrocatalyst for hydrazine electrooxidation. However, due to kinetic complexities, the electrooxidation of hydrazine still encounters overpotentials higher than 0.3 V; another difficulty is that hydrazine electrooxidation may also proceed *via* the so-called indirect pathway, corresponding to hydrogen generation (Eq. (2)) and its subsequent valorization (electrooxidation), or even by a faradic-inefficient pathway in which no electrons are generated, if hydrogen is not valorized.

$$N_2H_4 \rightarrow N_2 + 2H_2 \quad (2)$$

Therefore, the electrochemical oxidation of hydrazine received substantial attention in the past decades. Compton and Aldous [12] have evidenced that the onset potential of hydrazine electrooxidation was low on activated or partially oxidized Pt surfaces. However, Pt electrodes were prone to deactivation after holds at open circuit potential (OCP), which was associated to the hydrazine-induced reduction of the residual oxides. This finding shows the importance of surface oxides on the electrooxidation of adsorbed reaction intermediates. Asazawa and co-workers [6] demonstrated high electrochemical activity and stability for Ni in

* Corresponding author.
E-mail addresses: fabiohbl@iqsc.usp.br, fabiohbl@gmail.com (F.H.B. Lima).

http://dx.doi.org/10.1016/j.apcatb.2016.08.007
0926-3373/© 2016 Elsevier B.V. All rights reserved.

comparison to Co anodes towards hydrazine electrooxidation in direct hydrazine fuel cells (*i.e.* at large hydrazine concentration and temperature above $T = 60\,^{\circ}C$). However, this behavior depends on the operating conditions: Ni and Co both present low activities at low hydrazine concentrations and low temperature (*e.g.* $T = 25\,^{\circ}C$) [13]. In this context, there is still room to improve hydrazine electrooxidation catalysts. To that goal, electrocatalysts combining nickel and noble metals like platinum [14,15] or Pd [16], or nickel and non-noble metals [7,17–19], have shown high activity in half or single cells, operating with hydrazine in alkaline solution. Nevertheless, and particularly for the combination of Ni with Pt, there is a lack of knowledge about the dependence of the Ni-Pt composition *vs* electrocatalytic activity and reaction pathway.

Herein, considering that sites for dehydrogenation and superficial oxides are important in the electrooxidation of hydrazine [12], carbon-supported NiO_x-modified Pt nanoparticles were investigated as bi-element electrocatalysts for this reaction, and their activity was compared to that of carbon-supported Pt (Pt/C) and NiO_x (NiO_x/C) nanoparticles. The reaction products were monitored as a function of the electrode potential for the most active electrocatalyst, *via* on-line Differential Electrochemical Mass Spectrometry (DEMS) measurements.

2. Experimental

The carbon-supported Ni-modified Pt nanoparticles, represented as NiO_x-Pt/C, were prepared by impregnating Pt/C (20 wt.%, E-TEK) with $Ni(NO_3)_2{\cdot}2H_2O$, in aqueous solution, followed by thermal decomposition in air at 220 °C; three different Ni:Pt nominal atomic ratios were synthesized by adjusting the amount of Ni precursor: 85:15, 90:10, and 97:3. The NiO_x/C electrocatalyst was synthesized in a similar fashion, but now impregnating pure Vulcan carbon with $Ni(NO_3)_2{\cdot}2H_2O$, followed by thermal decomposition in air at 300 °C. The electrocatalyst phases were characterized by X-ray Diffraction (XRD) (Rigaku Multiflex—Ultima IV, Cu-Kα radiation), and the average crystallite sizes were estimated by using the Scherrer equation [20]. Transmission electron microscopy (TEM) images were obtained using a FEI TECNAI G^2 F20 (200 kV) equipment. The average particle diameters were measured by counting at least 400 particles on representative TEM micrographs using the ImageJ software. The nanoparticles were also analyzed in high-resolution scanning transmission electron microscopy – high-angle annular dark field (HRSTEM-HAADF) imaging mode. HRSTEM – X-Ray energy dispersive spectrometry (X-EDS) line scan measurements were also performed on some electrocatalyst domains to analyze the chemical composition and distribution of the atomic species in the vicinity of the Pt nanoparticles. The analyses were performed on the Pt L and the Ni K lines, using the K factor provided by the TIA software. Additionally, the overall atomic compositions of each electrocatalyst were determined by means of Atomic Absorption Spectroscopy, performed using a PinAAcle 900 F apparatus (PerkinElmer) piloted by the Syngistix software.

The electrochemical experiments were conducted in a jacketed cell, with controlled temperature at $T = 25\,^{\circ}C$, and using 1.0 mol L^{-1} NaOH as supporting electrolyte (Mallinckrodt Chemicals), in the absence or in the presence of 0.1 mol L^{-1} hydrazine hydrate (64 wt.%). A ring-shaped gold plate was used as counter-electrode, and $Hg/HgO/OH^-$ as reference electrode, respectively. However, all the potential values are expressed on the RHE scale. The working electrodes were prepared by depositing an aqueous suspension of the adequate electrocatalyst on the glassy carbon disk (0.3 mg cm^{-2}) of a rotating disk electrode [21], followed by the addition of a diluted Nafion® (0.05 wt%) solution (Aldrich). Cyclic voltammetry (CV), and chronoamperometry experiments were performed using an AUTOLAB PGSTAT 128N potentiostat.

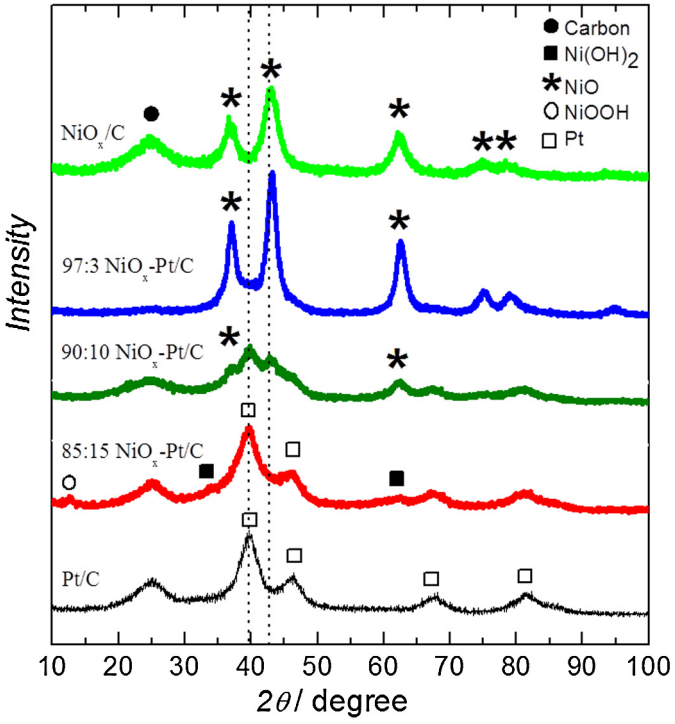

Fig. 1. X-ray powder diffraction intensities for the synthesized NiO_x-Pt/C nanoparticles with different Ni contents. The spectra obtained for NiO_x/C and Pt/C were included for comparison.

On-line DEMS measurements were performed with a Pfeiffer Vacuum QMA 200 quadrupole mass spectrometer using a setup consisting of two differentially pumping chambers. More details and features of this method are presented in previous publications [22,23]. The electrochemical cell was constructed following previously published principles [24]. For the DEMS measurements, the working electrodes were prepared in the form of a thin film by pipetting a total of 180 μL of an aqueous suspension (2.0 mg mL^{-1}) of the electrocatalyst (prepared in 1.0 mL of water + 50 μL of 5 wt.%, Nafion® solution) onto a carbon paper (Toray – Tacoma, WA, USA – TGP-H-060, 50 wt.% wet proofing), with 0.87 cm^{-2}, previously pressed with a Gore-Tex® PTFE membrane (pore size 0.02 μm). The hydrazine electrooxidation products were monitored at mass/charge ratios of: $m/z = 28$ (N_2), $m/z = 2$ (H_2), and $m/z = 15$ (NH_3).

3. Results and discussion

The XRD results, presented in Fig. 1, show the diffraction peaks obtained for the synthesized NiO_x-Pt/C electrocatalysts. The data obtained for NiO_x/C and Pt/C are included for comparison. It is observed the peaks associated to $Ni(OH)_2$, NiOOH, NiO for the sample with the lower Ni content (85:15), and, by increasing the Ni quantity, (90:10 and 97:3), it is noted a gradual raising of the diffraction peaks associated to the NiO phase, and a suppression (or masking) of the diffraction peaks of $Ni(OH)_2$, NiOOH and metallic Pt. Additionally, the comparison of the XRD patterns for the different NiO_x-Pt/C materials does not show a significant or appreciable alteration of the Pt and/or Ni lattice parameters (no alteration of the 2-theta positions in relation to those of the pure Pt or NiO phases): this evidences that the Ni phases are segregated from the Pt phase, instead of forming Ni-Pt alloys, which was anticipated and desired using this technique of catalyst synthesis, and that no metallic nickel is present in the as-prepared samples. The results of the electrocatalyst overall atomic compositions, determined by Atomic

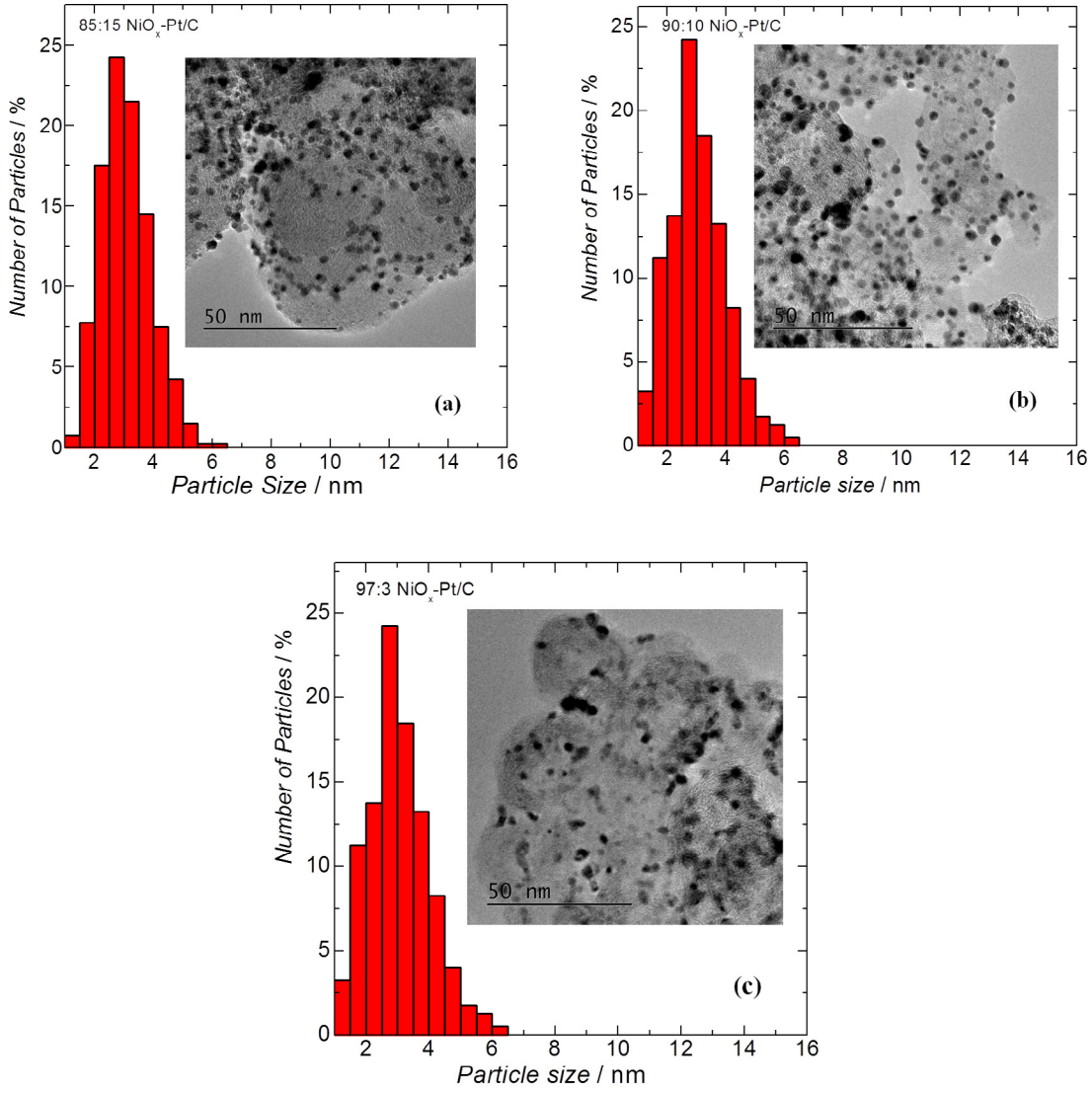

Fig. 2. High-resolution transmission electron microscopy images and their corresponding particle size distribution histograms for 85:15 (a), 90:10 (b), and 97:3 (c) NiO_x-Pt/C electrocatalysts.

Table 1
Nominal and determined electrocatalyst compositions, obtained by Atomic Absorption Spectroscopy. The atomic percents are related to the average of, at least, three different measurements.

NiO_x-Pt/C electrocatalyst (Nominal composition atom.%)	Loading (atom.%)	
	Ni	Pt
85:15	84.3 ± 1.6	15.7 ± 1.6
90:10	93.3 ± 0.1	6.7 ± 0.1
97:3	99.8 ± 0.2	0.2 ± 0.2

Absorption Spectroscopy, are presented in Table 1. It is observed that the atomic compositions are close to the nominal values, as it would be expected for an impregnation method of synthesis.

Fig. 2(a)–(c) shows the representative bright-field HRTEM images and the corresponding particle size distribution histograms for the synthesized NiO_x-Pt/C electrocatalysts with Ni:Pt atomic ratios of 85:15, 90:10, and 97:3, respectively. It is noted that the metallic particle dispersion on the carbon powder support is homogeneous and the histograms resulted in average particle sizes between 2.6 and 3.0 nm for the three different Ni:Pt compositions. Micrographs were also acquired in STEM-HAADF imaging mode to locate the Ni phases in relation to the Pt nanoparticles in the as-prepared samples. Fig. 3 shows the STEM-HAADF images and superposed X-EDS line scans for Pt and Ni contents for the various NiO_x-Pt/C samples (A, C, E), and the X-EDS maps in the corresponding regions for the Pt and Ni elements (B, D, F). In all cases, the XEDS signals show that Pt nanoparticles are surrounded by non-negligible amounts of Ni, the amount of Ni increasing in sequence 85:15 < 90:10 < 97:3 NiO_x-Pt/C, in agreement with the results from Atomic Absorption Spectroscopy (Table 1). More important, these data show that there is always Ni in the vicinities of the Pt nanoparticles, whatever the Ni load; this was desired and denotes for an intimate contact between these two metals. However, the Ni content in the 97:3 NiO_x-Pt/C sample is very (and probably too high), and one may anticipate that the abundant presence of nickel oxides may prevent accessibility to the sites of Pt in this case.

Fig. 4(a) shows the cyclic voltammograms of hydrazine electrooxidation obtained on the three different NiO_x-Pt/C electrocatalysts (Pt/C and NiO_x/C benchmarks were included for comparison; Fig. 4(b) presents a zoom on the onset potential domain for the investigated materials). It is observed that the presence of Ni-oxides in the 85:15 and 91:10 NiO_x-Pt/C electrocatalysts induces a remarkable acceleration of the hydrazine

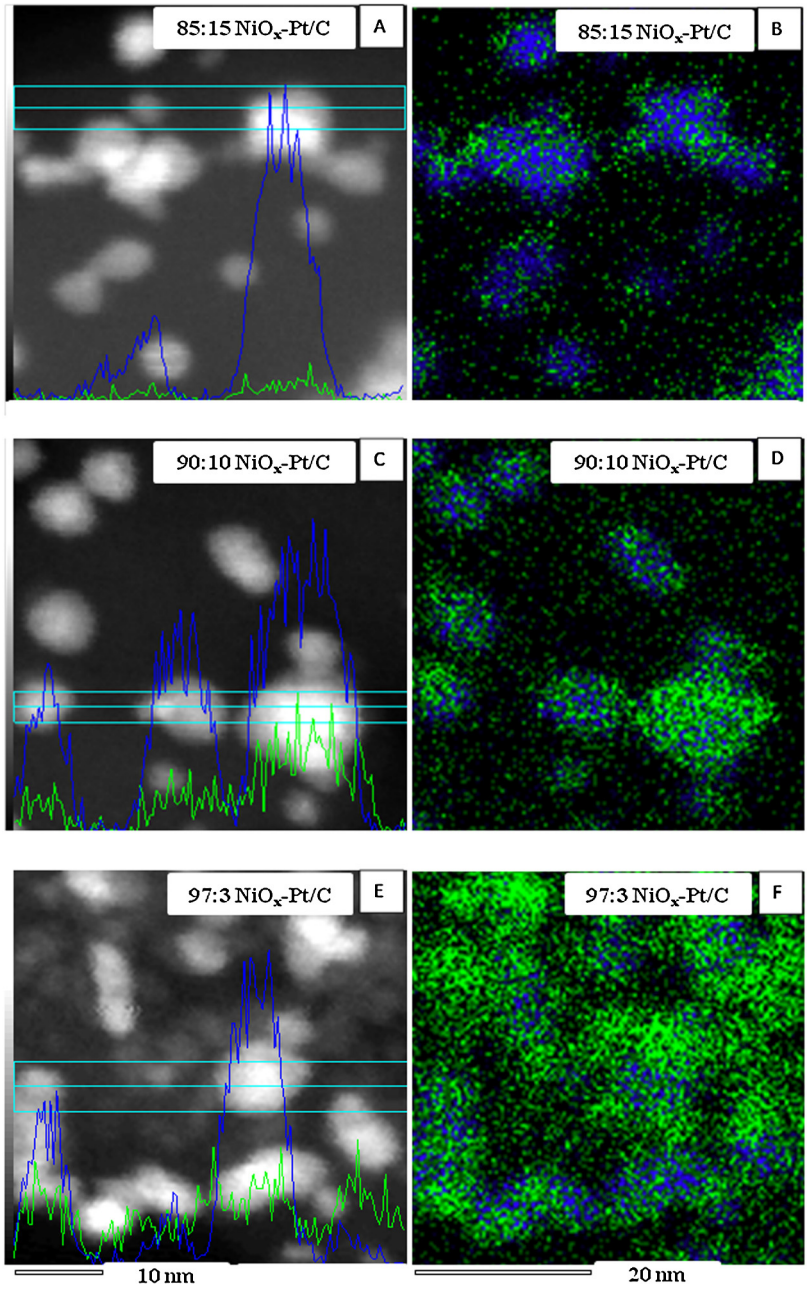

Fig. 3. STEM-HAADF image and superposed X-EDS line scan for Pt (blue) and Ni (green) contents for the various NiO_x-Pt/C samples (A, C, E); XEDS maps in the corresponding regions for the Pt (blue) and Ni (green) elements (B, D, F). In all cases, the X-EDS signals show that Pt nanoparticles are surrounded by non-negligible amounts of Ni, the amount of Ni increasing in sequence 85:15 NiO_x-Pt/C < 90:10 NiO_x-Pt/C < 97:3 NiO_x-Pt/C. (For interpretation of the references to color in this figure legend, the reader is referred to the web version of this article.)

electrooxidation at low potentials, in comparison to both pure Pt/C and pure NiO_x/C. According to the current onsets, the following order of activity can be drawn: 85:15 NiO_x-Pt/C > 90:10 NiO_x-Pt/C > pure Pt/C > 97:3 NiO_x-Pt/C > pure NiO_x/C (NiO_x/C presents marginal activity at this temperature and hydrazine concentration); this trend is presented as a Volcano plot in Fig. 4(c). Comparing the faradaic currents obtained during potentiostatic hydrazine electrooxidation experiments for 85:15 NiO_x-Pt/C and pure Pt/C (not shown here), it is demonstrated that the higher activity of the former remains when the potential is stepped from OCP to 0.22 V. Therefore, the activity enhancement brought by Ni-oxides adjunction to Pt/C does not vanish in near-steady-state conditions, which demonstrates that the electrocatalyst is not severely deactivated in these conditions. The authors point out that this result does not demonstrate the materials durability of the electrocatalyst, which has not been surveyed so far.

Fig. 5 presents the faradaic and ionic currents obtained in DEMS during cyclic voltammetry of hydrazine electrooxidation on the 85:15 NiO_x-Pt/C electrocatalyst (the most active sample). Hydrazine is catalytically decomposed on Pt and/or Ni-oxide surface at OCP into $N_2 + H_2$ (Eq. (2)) [25,26]. It is possible, as discussed below, that the H_2 generation proceeds *via* the dissociative adsorption of hydrazine onto the catalysts surface, that produce H_{ad}, which can further combine into H_2 at OCP [27,28] (and/or due to the coupling of the water electro-reduction and hydrazine electrooxidtion, as discussed below). The hydrazine oxidation reaction onset potential (faradaic current generation at *ca.* 0.02 V, Fig. 5(a)) coincides with the decrease in the H_2 and N_2 signals (or decelerated

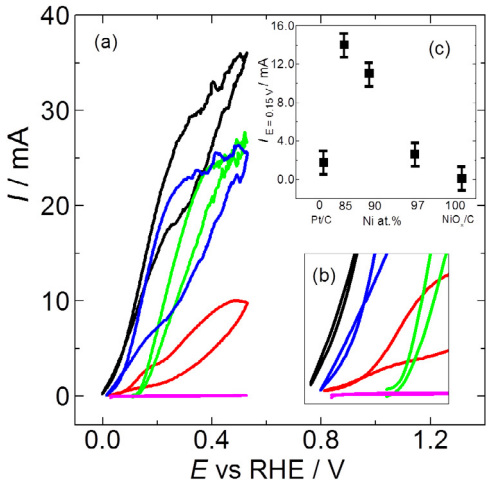

Fig. 4. Faradaic currents (without IR drop correction) obtained during cyclic voltammetry measurements of hydrazine electrooxidation catalyzed by the investigated NiO_x-Pt/C electrocatalysts, 85:15 (black), 90:10 (blue), and 97:3 (red) in 0.1 mol L^{-1} N_2H_4 + 1.0 mol L^{-1} NaOH solution. Sweep rate of 20 mV s^{-1} and temperature of 60 °C. NiO_x/C (pink) and Pt/C (green) were included for comparison (a); Zoom in of the low overpotential domain (b); Plot of the electrocatalytic activity ($I_{E=0.15\,V}$) *versus* Ni content for the different investigated electrocatalysts (c). (For interpretation of the references to color in this figure legend, the reader is referred to the web version of this article.)

formation of these species) (Fig. 5(b) and (c)). The electrooxidation of the produced H_2 and, possibly, H_{ad} contributes to the overall faradaic current, in similar manner as noted for the BOR [27,28], which may also influence the reduction of the H_2 signal. At slightly higher potential values (*ca.* 0.17 V), the ionic current corresponding to the N_2 production increases sharply (Fig. 5(c)), together with a faster reduction in the rate of H_2 detection (Fig. 5(b)) that defines a plateau at higher potentials. This indicates, at least, a parallel route of complete hydrazine electro-oxidation. Besides to the H_2 consumption *via* electrooxidation, the decrease in the H_2 mass signal signs that the residence time of the H_{ad} species at the NiO_x-Pt surface becomes minimal because the recombination of H_{ad} + H_{ad} becomes less and less possible as the potential increases due to their electrooxidation by OH_{ads}. Additionally, as numerically calculated [27] and experimentally measured [29] for the case of borohydride, the generated H_2 and N_2 at OCP can also come from de water electro-reduction, Eq. (3), that couples with the hydrazine electrooxidation on separate or on the same active site. As soon as the potential is increased, the water electro-reduction step is decelerated and, so, the overall hydrolysis decelerates, also accounting for the reduced rate of H_2 and N_2 formation at potentials above *ca.* 0–0.02 V.

$$H_2O + 2e^- = H_2 + OH^- \quad (3)$$

Furthermore, knowing that this mechanism proceeding with the dissociative adsorption of hydrazine with the valorization of H_{ad} is very site consuming, and that the DEMS data clearly show

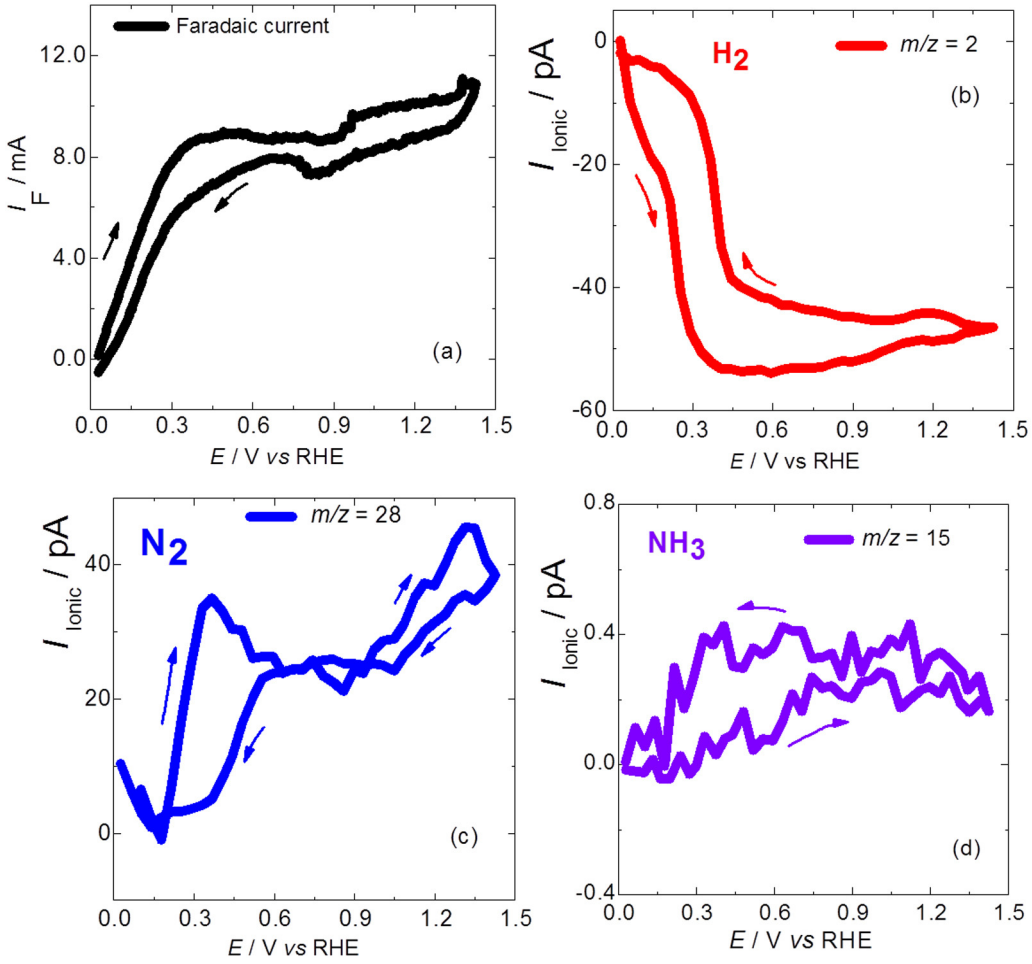

Fig. 5. Faradaic (a) and ionic currents for m/z = 2 (H_2) (b), m/z = 28 (N_2) (c), and m/z = 17 (NH_3) (d), obtained during DEMS experiments of cyclic voltammetry on 85:15 NiO_x-Pt/C in 0.1 mol L^{-1} hydrazine + 1.0 mol L^{-1} KOH electrolyte at 25 °C. Scan rate of 20 mV s^{-1}. For the mass signal, the values (or position) of the ionic currents at the OCP was taken as zero (baseline).

two regimes of oxidation, below and above *ca.* 0.17 V, the direct oxidation of hydrazine (without the step of dissociative adsorption) cannot be excluded in that "high-potential" region. Besides, in addition to hydrazine complete dissociative adsorption and electrooxidation pathway, a second pathway generating NH_3 (Fig. 5(d)) is detected to a minor extent at and above the OCP; it may occur following Eq. (4) and can initiate by the incomplete dissociation of hydrazine or *via* another route, which will be given below.

$$3N_2H_4 \rightarrow N_2 + 4NH_3 \quad (4)$$

The increased apparent activity for hydrazine oxidation with Ni-oxide adjunction to Pt points toward an interplay of Ni-oxides and Pt atoms for the hydrazine electrooxidation reaction at low potentials, and this seems to be a bifunctional effect [30]. It can be suggested that hydrazine electrooxidation reaction on NiO_x-Pt/C electrocatalysts occurs in the following steps: (i) Pt atoms promote the dissociative adsorption of hydrazine into adsorbed hydrogen (Pt–H_{ads}) and nitrogen (N_2) (Eq. (5)); (ii) NiO_x species present in the as-synthesized electrocatalysts, at low potential and at low hydrazine concentration, are reduced to a mixed $Ni^0/Ni(OH)_2$ phase, but with much higher amount of $Ni(OH)_2$; this also means that Ni allows the OH^- discharge at low potentials producing Ni–OH_{ads} species (the $Ni(OH)_2$ phase) [31] (Eq. (6)); eventually, (iii) Ni–OH_{ads} and Pt–H_{ads} combine into water (Eq. (7)). Here, it is worth mentioning that the full process of hydrazine electrooxidation (dehydrogenation and H_{ads}–OH_{ads} coupling) may also take place on the $Ni^0/Ni(OH)_2$ surface of a pure Ni electrocatalyst. Nevertheless, for low values of hydrazine concentrations (~0.1 mol L^{-1} Fig. 4a), the Ni-hydroxide is the major phase [32], and this surface is less active than a mixed $Ni^0/Ni(OH)_2$ surface with similar quantities of metallic nickel and nickel hydroxide. This was also evidenced by the electrochemical measurements associated with *in situ* XAS results of Ref. [31]. A surface with significant amount of Ni^0 may be obtained from the depassivation of nickel-based catalysts, close to the OCP, when the hydrazine concentration is large enough to drag the potential negative enough, and this may explain the high activity of Ni at higher hydrazine concentrations; (it is also possible the full depassivation of Ni by incursions to very low potential, but this was not attempted here). In the present low hydrazine concentrations (and for electrode potentials that in all cases were maintained above 0 V), at OCP, the resulting phase is basically formed by nickel hydroxide, and, so, the full electrooxidation of hydrazine occurring only on this nearly pure Ni-hydroxide phase contributes only to a minor extent to the overall faradaic current. This is because in the hydrazine oxidation mechanism, one needs metal sites for the dissociative adsorption of hydrazine into H_{ad}, and oxide sites for the oxidation/stripping of the H_{ad}; as in the case of the oxidation of BH_4^- on Pt [27].

In that context, the electrooxidation of hydrazine on the bimetallic NiO_x-Pt/C material requires an optimal interplay between the exposed active sites of Pt (for the dissociative adsorption of hydrazine) and Ni (to provide OH_{ad} species at low potential and to enable the complete H_{ad} oxidation). The Ni coverage brought by the 85:15 atomic ratio exhibits the best balance and overall activity; on the contrary, the highest Ni load (97:3) considerably decreases the number of superficial Pt active sites, which hinders the dissociative adsorption of hydrazine and decreases the overall reaction rate.

Considering the above-exposed scenario, the faradic current obtained at low potential results from the oxidation of H_{ad} and H_2 species (depending on the value of H_{ad} coverage, H_2 may evolve and be detected in DEMS). In both cases, these species are produced *via* hydrazine dissociative adsorption (dehydrogenation), and further electrooxidized by OH_{ads} species, according to Eqs. (5)–(8).

$$N_2H_4 = 4H_{ad} + N_2 \quad \text{likelyonPt(requires5Ptsites)} \quad (5)$$

$$OH^- = OH_{ad} + e^- \quad \text{likelyonNiatoms/oxides} \quad (6)$$

$$H_{ads} + OH_{ad} = H_2O \quad \text{attheinterfacebetweenPtandNi-xoide} \quad (7)$$

$$H_{ads} + H_{ads} = H_2 \quad \text{likelyonPt, atlarge}H_{ad}\text{coverage} \quad (8)$$

Therefore, the presence of Ni, which accelerate/facilitate the OH^- discharge into OH_{ads} (Eq. (5)) at lower potential than that on Pt, render the H_{ads} conversion into water easier (Eq. (6)) and, overall, facilitates the electrooxidation of hydrogen species; this process agrees with that proposed by Markovic and co-authors for the hydrogen electrooxidation on $Ni(OH)_2$-decorated Pt(111) electrodes [33], and may explain the higher activity of the synthesized NiO_x-Pt/C when compared to pristine Pt/C. Above *ca.* 0.17 V, OH_{ad} start to form also at the Pt surface, and the direct oxidation of hydrazine can take place. However, when the potential gets to high (typically above 0.62 V on the positive going scan of Fig. 5), Pt oxides start to form, and the dissociative adsorption of hydrazine + valorization of H_{ad} (very site-consuming) compete with the chemical generation of ammonia at metal oxides (Eq. (4)), which is the result of a mixed reaction between the oxidation of hydrazine at the bare metal surface (Eq. (1)) and the reduction of hydrazine at the sites of oxidized metal surface (Eq. (9)) [34].

$$N_2H_4 + 2H_2O + 2e^- = 2NH_3 + 2OH^- \quad \text{likelyonoxides} \quad (9)$$

The fact that, overall, the faradaic efficiency is lower on the negative scan in Fig. 5 than on the positive one militates in favor of the detrimental influence of surface hydroxides/oxides (their reduction proceeds at lower potential than their formation). This illustrates the dual role of surface hydroxides/oxides in the mechanism of hydrazine hydrate oxidation reaction, as was put into evidence for the BOR at Pt electrodes [27]: although OH_{ad} are required to complete the oxidation of the H_{ad} species formed from the dissociative adsorption of N_2H_4, there must remain some extent of oxide-free Pt surface to promote the dissociative adsorption of hydrazine (Eq. (5), very site-consuming). In that extent, NiO_x-Pt composite surfaces, with low surface fraction of Ni, are better catalysts than Pt, because they optimize this interplay between the oxophilic and noble sites, thereby favoring a bifunctional hydrazine oxidation pathway.

4. Conclusion

NiO_x-modified Pt/C nanocomposites showed much lower onset potential in comparison to that of pure Pt/C or NiO_x/C. This was explained by the occurrence of a bifunctional mechanism, in which OH_{ad} species on Ni sites assists the oxidation of adsorbed H_{ad} on the Pt surface. On-line DEMS results showed that NiO_x-Pt/C catalyzes the heterogeneous chemical decomposition of hydrazine at OCP (dissociative adsorption), producing H_2 and N_2. At potentials above the OCP, the H_2 DEMS signal decreased concomitantly with the increase in faradaic current, and this was due to H_2 (and H_{ad}) consumption *via* electrochemical oxidation on Pt, or due to deceleration of the hydrolysis route by the suppression of the water electro-reduction. At slightly higher potential values, the N_2 signal raised fast, indicating the onset of complete dehydrogenation/electrooxidation of hydrazine. A slight ionic signal of NH_3 was evident on the whole potential domain, suggesting that a minor route of incomplete hydrazine dissociative adsorption (low potential) and electrooxidation (high potential) proceeds.

Acknowledgements

The authors gratefully acknowledge financial support from FAPESP (Fundação de Amparo à Pesquisa do Estado de São Paulo) – Sao Paulo Research Foundation – FHBL – Grant Nos. 2011/50727-9 and 2013/16930-7 and DCO – Grants: 2013/12232-3 and 2013/00197-9; CAPES-COFECUB (Project No. Ph598/08); CNPq

(Conselho Nacional de Desenvolvimento Científico e Tecnológico) – FHBL – Grant Nos. 306213/2013-3 and 477153/2013-5. WOS and FHBL thank Fundação de Amparo à Pesquisa do Estado do Maranhão – Maranhao Research Foundation – Grant No. BD-01638/13. MC thanks the French IUF.

References

[1] D.X. Cao, D.D. Chen, J. Lan, G.L. Wang, J. Power Sources 190 (2009) 346–350.
[2] X. Yan, F. Meng, Y. Xie, J. Liu, Y. Ding, Sci. Rep. 2 (2012) 941–947.
[3] S.C. Amendola, P. Onnerud, M.T. Kelly, P.J. Petillo, S.L. Sharp-Goldman, M. Binder, J. Power Sources 84 (1999) 130–133.
[4] P.-Y. Olu, F. Deschamps, G. Caldarella, M. Chatenet, N. Job, J. Power Sources 297 (2015) 492–503.
[5] X.-B. Zhang, S. Han, J.-M. Yan, M. Chandra, H. Shioyama, K. Yasuda, N. Kuriyama, T. Kobayashi, Q. Xu, J. Power Sources 168 (2007) 167–171.
[6] K. Asazawa, K. Yamada, H. Tanaka, A. Oka, M. Taniguchi, T. Kobayashi, Angew. Chem. Int. Ed. 46 (2007) 8024–8027.
[7] A. Serov, M. Padilla, A.J. Roy, P. Atanassov, T. Sakamoto, K. Asazawa, H. Tanaka, Angew. Chem. Int. Ed. 53 (2014) 10336–10339.
[8] H. Tanaka, K. Asazawa, T. Sakamoto, T. Kato, M. Kai, S. Yamaguchi, K. Yamada, H. Fujikawa, ECS Trans. 16 (2008) 459–464.
[9] Q. Yi, H. Chu, M. Tang, Y. Zhang, X. Liu, Z. Zhou, H. Nie, Fuel Cells 14 (2014) 827–833.
[10] S. Yamazaki, Z. Siroma, N. Fujiwara, M. Asahi, K. Asazawa, H. Tanaka, T. Ioroi, Electrochim. Acta 94 (2013) 38–41.
[11] S.-i. Yamazaki, K. Kuratani, H. Senoh, Z. Siroma, K. Yasuda, J. Power Sources 195 (2010) 1107–1111.
[12] L. Aldous, R.G. Compton, Phys. Chem. Chem. Phys. 13 (2011) 5279–5287.
[13] D.C. Oliveira, M. Chatenet, F.H.B. Lima, in preparation (2016).
[14] S.J. Lao, H.Y. Qin, L.Q. Ye, B.H. Liu, Z.P. Li, J. Power Sources 195 (2010) 4135–4138.
[15] Y. Ma, H. Wang, W. Lv, S. Ji, B.G. Pollet, S. Li, R. Wang, RSC Adv. 5 (2015) 68655–68661.
[16] L.Q. Ye, Z.P. Li, H.Y. Qin, J.K. Zhu, B.H. Liu, J. Power Sources 196 (2011) 956–961.
[17] U. Martinez, K. Asazawa, B. Halevi, A. Falase, B. Kiefer, A. Serov, M. Padilla, T. Olson, A. Datye, H. Tanaka, P. Atanassov, Phys. Chem. Chem. Phys. 14 (2012) 5512–5517.
[18] T. Sakamoto, K. Asazawa, U. Martinez, B. Halevi, T. Suzuki, S. Arai, D. Matsumura, Y. Nishihata, P. Atanassov, H. Tanaka, J. Power Sources 234 (2013) 252–259.
[19] T. Sakamoto, K. Asazawa, J. Sanabria-Chinchilla, U. Martinez, B. Halevi, P. Atanassov, P. Strasser, H. Tanaka, J. Power Sources 247 (2014) 605–611.
[20] B.D. Cullity, S.R. Stock, Elements of X-Ray Diffraction, 3rd ed., Upper Saddle River, USA (2001).
[21] T.J. Schmidt, H.A. Gasteiger, G.D. Stab, P.M. Urban, D.M. Kolb, R.J. Behm, J. Electrochem. Soc. 145 (1998) 2354–2358.
[22] A.C. Queiroz, W.O. Silva, I.A. Rodrigues, F.H.B. Lima, Appl. Catal. B: Environ. 160–161 (2014) 423–435.
[23] E.B.C. Bittins-Cattaneo, P. Konigshoven, W. Vielstich, Electroanalytical Chemistry—A Series of Advances, New York (1991).
[24] R. Ianniello, V.M. Schmidt, Ber. Bunsen Ges. Phys. Chem. 99 (1995) 83–86.
[25] J. Sanabria-Chinchilla, K. Asazawa, T. Sakamoto, K. Yamada, H. Tanaka, P. Strasser, J. Am. Chem. Soc. 133 (2011) 5425–5431.
[26] Y.J. Zhong, H.B. Dai, Y.Y. Jiang, D.M. Chen, M. Zhu, L.X. Sun, P. Wang, J. Power Sources 300 (2015) 294–300.
[27] P.Y. Olu, A. Bonnefont, M. Rouhet, S. Bozdech, N. Job, M. Chatenet, E. Savinova, Electrochim. Acta 179 (2015) 637–646.
[28] A.M. Pasqualeti, P.Y. Olu, M. Chatenet, F.H.B. Lima, ACS Catal. 5 (2015) 2778–2787.
[29] Z. Jusys, R.J. Behm, Electrochem. Commun. 60 (2015) 9–12.
[30] M. Watanabe, S. Motoo, J. Electroanal. Chem. 60 (1975) 267–273.
[31] T. Sakamoto, D. Matsumura, K. Asazawa, U. Martinez, A. Serov, K. Artyushkova, P. Atanassov, K. Tamura, Y. Nishihata, H. Tanaka, Electrochim. Acta 163 (2015) 116–122.
[32] D.A. Finkelstein, R. Imbeault, S. Garbarino, L. Roue, D. Guay, J. Phys. Chem. C 120 (2016) 4717–4738.
[33] R. Subbaraman, D. Tripkovic, D. Strmcnik, K.C. Chang, M. Uchimura, A.P. Paulikas, V. Stamenkovic, N.M. Markovic, Science 334 (2011) 1256–1260.
[34] T. Kodera, M. Honda, H. Kita, Electrochim. Acta 30 (1985) 669–675.